pH- and NIR Light-Responsive Micelles with Hyperthermia-Triggered Tumor Penetration and Cytoplasm Drug Release to Reverse Doxorubicin Resistance in Breast Cancer

Haijun Yu, Zhirui Cui, Pengcheng Yu, Chengyue Guo, Bing Feng, Tongying Jiang, Siling Wang, Qi Yin, Dafang Zhong, Xiangliang Yang, Zhiwen Zhang, and Yaping Li**

The acquisition of multidrug resistance (MDR) is a major hurdle for the successful chemotherapy of tumors. Herein, a novel hybrid micelle with pH and near-infrared (NIR) light dual-responsive property is reported for reversing doxorubicin (DOX) resistance in breast cancer. The hybrid micelles are designed to integrate the pH- and NIR light-responsive property of an amphiphilic diblock polymer and the high DOX loading capacity of a polymeric prodrug into one single nanocomposite. At physiological condition (i.e., pH 7.4), the micelles form compact nanostructure with particle size around 30 nm to facilitate blood circulation and passive tumor targeting. Meanwhile, the micelles are quickly dissociated in weakly acidic environment (i.e., pH ≤ 6.2) to release DOX prodrug. When exposed to NIR laser irradiation, the hybrid micelles can trigger notable tumor penetration and cytosol release of DOX payload by inducing tunable hyperthermia effect. In combination with localized NIR laser irradiation, the hybrid micelles significantly inhibit the growth of DOX-resistant MCF-7/ADR breast cancer in an orthotopic tumor bearing mouse model. Taken together, this pH and NIR light-responsive micelles with hyperthermia-triggered tumor penetration and cytoplasm drug release can be an effective nanoplatform to combat cancer MDR.

1. Introduction

Breast cancer is the most common malignant tumor and the second-leading cause for high mortality in female cancer patients.[1] For clinical treatment of breast cancer, systemic chemotherapy after surgical resection of the primary tumor is one important option.[2,3] Unfortunately, the therapeutic efficacy of chemotherapy is severely impeded by the occurrence of acquired multidrug resistance (MDR) in cancer cells, which has been defined as the main obstacle for the success of chemotherapy.[4] Two important causes could account for the occurrence of acquired cancer MDR, one is the insufficient drug delivery throughout the tumor, the another could be continually exposing of cancer cells to a sublethal dose of anticancer drugs.[5–7]

In the last decade, the nanodrug delivery systems (NDDS) with either passive or active tumor targeting ability have gained extensive attention for combating cancer MDR.[8,9] The NDDS could not only elongate the blood circulation of small molecular drugs but also passively increase the tumoral accumulation of anticancer drugs via enhanced tumor penetration and retention (EPR) effect.[10–12] Despite all these well-known advantage of NDDS over their small molecular counterparts, many of current NDDS were prepared by noncovalently encapsulating the hydrophobic drugs inside the nanoparticle core.[13,14] Thus the drug loading ratio in these nanoparticles was usually unsatisfied, and drug leakage from the nanoparticles was unavoidable during blood circulation.[15,16] Moreover, the intratumoral diffusion of these conventional nanoparticles might be very inefficient due to the presence of extracellular barriers even they successfully bring the chemotherapeutic payload to the tumor site.[17,18] The dense extracellular matrix and absence of lymphatic drainage system of solid tumor could synergistically induce a reduced transcapillary pressure gradient and an elevated interstitial fluid pressure, thus restrict the nanoparticle only in the perivascular areas of the tumor tissue. The limited tumor penetration of nanoparticles could be improved to some extend by reducing the particle size,[19] or using multistage larger nanoparticles to transport and unload smaller ones

Dr. H. Yu, Z. Cui, P. Yu, C. Guo, B. Feng, Dr. Q. Yin, Dr. Z. Zhang, Prof. Y. Li
State Key Laboratory of Drug Research and Center of Pharmaceutics
Shanghai Institute of Materia Medica
Chinese Academy of Sciences
Shanghai 201203, P.R. China
E-mail: hjyu@simm.ac.cn; ypli@simm.ac.cn

Z. Cui, T. Jiang, S. Wang
School of Pharmacy
Shenyang Pharmaceutical University
Shenyang 110016, P.R. China

P. Yu, X. Yang
National Engineering Research Center for Nanomedicine
College of Life Science and Technology
Huazhong University of Science and Technology
Wuhan 430074, P.R. China

Prof. D. Zhong
State Key Laboratory of Drug Research and Center for Drug Metabolism
Shanghai Institute of Materia Medica
Chinese Academy of Sciences
Shanghai 201203, P.R. China

DOI: 10.1002/adfm.201404484

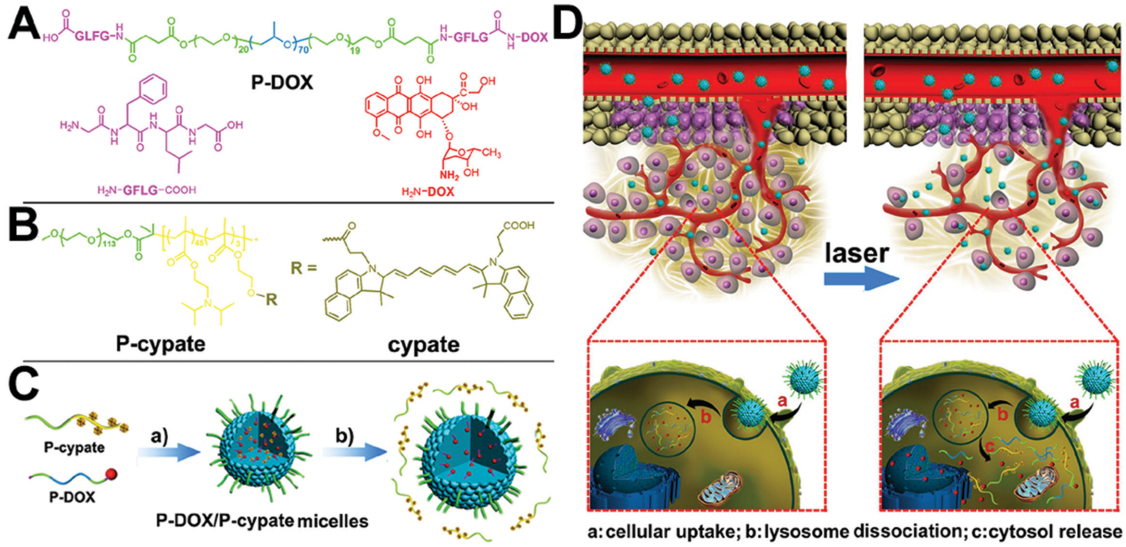

Figure 1. Chemical structures of A) DOX prodrug (P-DOX) and B) P-cypate diblock copolymer. C) Self-assembly structure of pH and NIR light dual-responsive P-DOX/P-cypate micelles: a) P-DOX and P-cypate diblock copolymer formed self-assemble micelles at physiological pH; b) the micelles dissociated at acidic condition due to protonation of PDPA tertiary amino groups. D) Scheme illumination for combating cancer MDR using the pH and NIR light dual-responsive P-DOX/P-cypate micelles. The micelles could passively accumulate in tumor organ via "EPR" effect. NIR laser irradiation following systemic injection of the hybrid micelles induced moderate hyperthermia effect by converting the photo energy to local heat, thus disrupted the dense extracellular matrix and lysosome membrane to facilitate tumor penetration and cytoplasm release of DOX payload.

at the tumor site.[20] Furthermore, the accumulated evidences indicated that MDR cancer cells contain a larger number of lysosomes with more acidic environment than their parental counterparts as a mean of cancer cell defense against chemotoxins.[21,22] The drug-loaded nanoparticles or weakly basic chemotherapeutics (i.e., doxorubicin, DOX) were therefore sequestrated inside the lysosome vesicles of the MDR cancer cells, and eventually eliminated from the cancer cells through increased activity of the secretory pathway.[23,24] Taken together, overcoming all these extracellular and cellular barriers to achieve uniform tumoral penetration and timely cytosol release of drug-loaded nanoparticles remains a challenge for NDDS to treat MDR breast cancer.

We had previously reported a set of poly(diisopropanolamino ethyl methacrylate) (PDPA) based polymeric nanoparticles for highly efficient delivery of small interfering RNA (siRNA),[25] photosensitizer,[26] and anticancer drug.[27] These nanoparticles could be specifically dissociated in early endosomes for payload release due to protonation of PDPA core. Herein, to address the limited tumor penetration and lysosome sequestration of nanoparticle drugs, and prevent drug leakage during blood circulation, a novel pH and NIR light dual-responsive micelle loading DOX prodrug was designed and its potential for combating DOX resistance in breast cancer was exploited. The micelle was prepared from a pluronic copolymer P123 conjugated DOX prodrug (P-DOX) and cypate-conjugated poly(ethylene glycol)-block-poly(diisopropanolamino ethyl methacrylate) (PEG-*b*-PDPA) diblock copolymer (P-cypate), hereinafter referred as P-DOX/P-cypate. The pH-responsive PEG-*b*-PDPA diblock copolymer was endowed with a NIR light responsive property by grafting with a NIR dye cypate. It was expected that the P-DOX/P-cypate micelles could keep their structural integrity during blood circulation, while be dissociated in weakly acidic endosomes to release P-DOX payload. Moreover, localized NIR laser irradiation following systemic administration of the dual-responsive micelles could trigger the tumor penetration and cytoplasm release of DOX payload by inducing a hyperthermia effect, thus the DOX resistance in MDR breast cancer could be reversed (**Figure 1**).

2. Results and Discussion

2.1. Preparation and Characterization of P-DOX/P-Cypate Hybrid Micelles

The P-DOX was synthesized by conjugating DOX to a pluronic triblock copolymer P123 via a tetrapeptide spacer glycine-phenylalanine-leucine-glycine (GFLG) (Figures 1A and SI1, Supporting Information). Pluronic P123 was selected as a precursor for prodrug synthesis because it is of amphiphilic property and able to suppress P-gp activation by depleting adenosine triphosphate (ATP) production.[28,29] The GFLG is specific for lysosome enzyme cleavage[30,31] Thus, after cellular uptake of the P-DOX/P-cypate micelles, DOX could be released from P-DOX in lysosome. In the meanwhile, P123 liberated from the prodrug was expected to inhibit drug efflux by inactivating P-gp protein. Each P123 molecular was conjugated with one DOX, and a DOX conjugation ratio of 7.5 wt% was found in the resultant P-DOX as estimated by fluorescence spectroscopic measurement. In parallel, cypate with high photothermal conversion efficacy in the NIR region[32] was grafted on the pendant hydroxyl groups of PEG-*b*-PDPA diblock copolymer via ester bonds (Figures 1B and SI2, Supporting Information). Each diblock copolymer was conjugated with three cypate molecule. The cypate weight percentage in the resultant copolymer

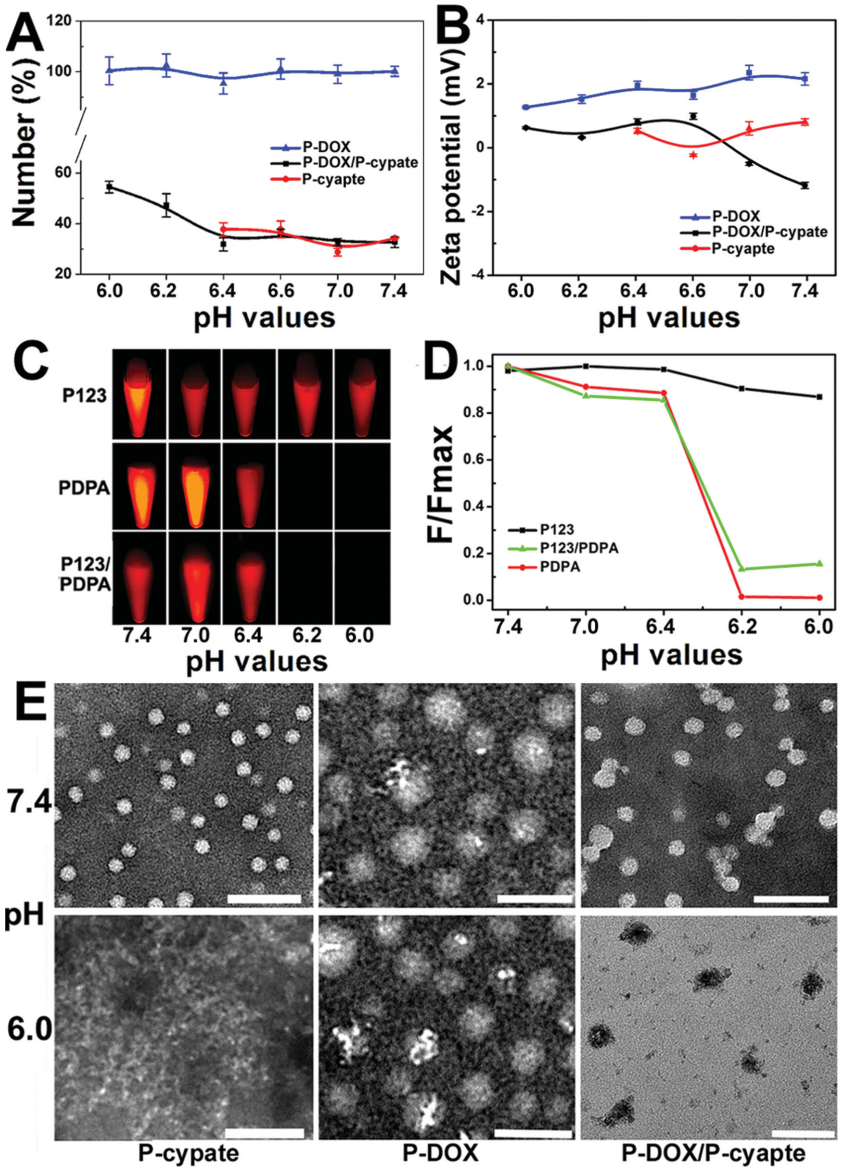

Figure 2. Characterization of the pH-responsive properties of P-DOX/P-cypate hybrid micelles. Change of A) hydrodynamic particle size and B) zeta-potential of the hybrid nanoparticles in response to buffer pHs. C) The fluorescent images and D) fluorescence quenching profile of NR-loaded P123/PDPA micelles at different pH condition, respectively. E) TEM images of P-capyte, P-DOX, and P-DOX/P-cypate micelles measured at neutral (i.e., pH 7.4) or acidic (i.e., pH 6.0) pH condition (scale bar 100 nm).

was 12 wt% determined using UV–vis spectroscopic measurement. Afterwards, P-DOX/P-cypate hybrid micelles were prepared using a solvent-precipitation method (Figure 1C).

The pH-responsive property of the hybrid micelles was first examined by dynamic light scattering (DLS) and zeta-potential measurements for particle size and surface charge, respectively. The particle size of P-DOX loaded nanoparticles kept almost the same disregarding pH change, implying a pH insensitive property of P-DOX (**Figure 2**A). The particle size of P-DOX/P-cypate and P-cypate micelles changed differently. At pH ≥ 6.4, the particle size of either P-DOX/P-cypate micelles or P-cypate controls were kept unchanged. At pH below 6.2, no P-cypate micelles were detected by DLS measurement because protonation of PDPA segment and dissociation of the hybrid micelles. In contrast, P-DOX/P-cypate micelles swelled from 32 ± 0.2 nm at pH 7.4 to 54 ± 2.3 nm at pH 6.0 (Figure S3, Supporting Information). Neutral surface charge was found for P-DOX/P-cypate micelles in the pH buffers ranging from 6.0 to 7.4 (Figure 2B). We thus estimated that P-cypate diblock copolymer dissociated from the hybrid micelles upon protonation in acidic environment (i.e., pH ≤ 6.2) since a positive surface charge should be detected if the protonated P-cypate molecules retained in the hybrid micelles. The acidic pH-triggered disassembly of hybrid-DOX/P-cypate micelles was further examined by fluorescent measurement. To do that, P123/PDPA micelles were loaded with nile red (NR), a polarity-responsive while pH insensitive fluorescent dye.[33] DOX and cypate-free micelles were prepared to avoid interfering with the fluorescent signal of NR. As shown in Figure 2C,D, at pH > 6.4, strong fluorescence emission assigned to NR was detected in the solution of PDPA, P123 or P123/PDPA micelles due to encapsulation of NR in the hydrophobic micelle core. At pH ≤ 6.2, the fluorescent signal of PDPA and P123/PDPA micelles was completely quenched due to micelle dissociation and NR release into the aqueous phase. The acid-induced dissociation of P-DOX/P-cypate micelles was confirmed by transmission electron microscopic (TEM) measurement. At pH 7.4, both P-cypate and P-DOX/P-cypate micelles were of spherical morphology with particles size around 30 nm. At acidic pH 6.0, P-DOX/P-cypate micelles dissociated and reformed amorphous P-DOX aggregates with particle size around 50 nm as found by DLS and fluorescence spectroscopic measurements (Figure 2E).

In order to induce hyperthermia effect with NIR laser irradiation, we used cypate as a NIR light-responsive component in this study. Thus we examined the UV–vis/fluorescence spectroscopic and photothermal conversing properties of P-DOX/P-cypate micelles. As shown in **Figure 3**A,B, both P-cypate and P-DOX/P-cypate mixture in dimethyl sulfoxide (DMSO) solution displayed strong UV–vis absorbance peak at ≈790 nm, which could be assigned to the specific photoabsorbance of cypate. In aqueous solution with pH 7.4, a greatly broadened absorbance band with moderate intensity was observed for P-cypate and P-DOX/P-cypate micelles in the region of 650–850 nm, due to micelle formation and cypate aggregation inside the hydrophobic PDPA core. The UV–vis absorbance was not recovered when the buffer pH was reduced from 7.4 to 5.8, although both kinds of micelles dissociated completely

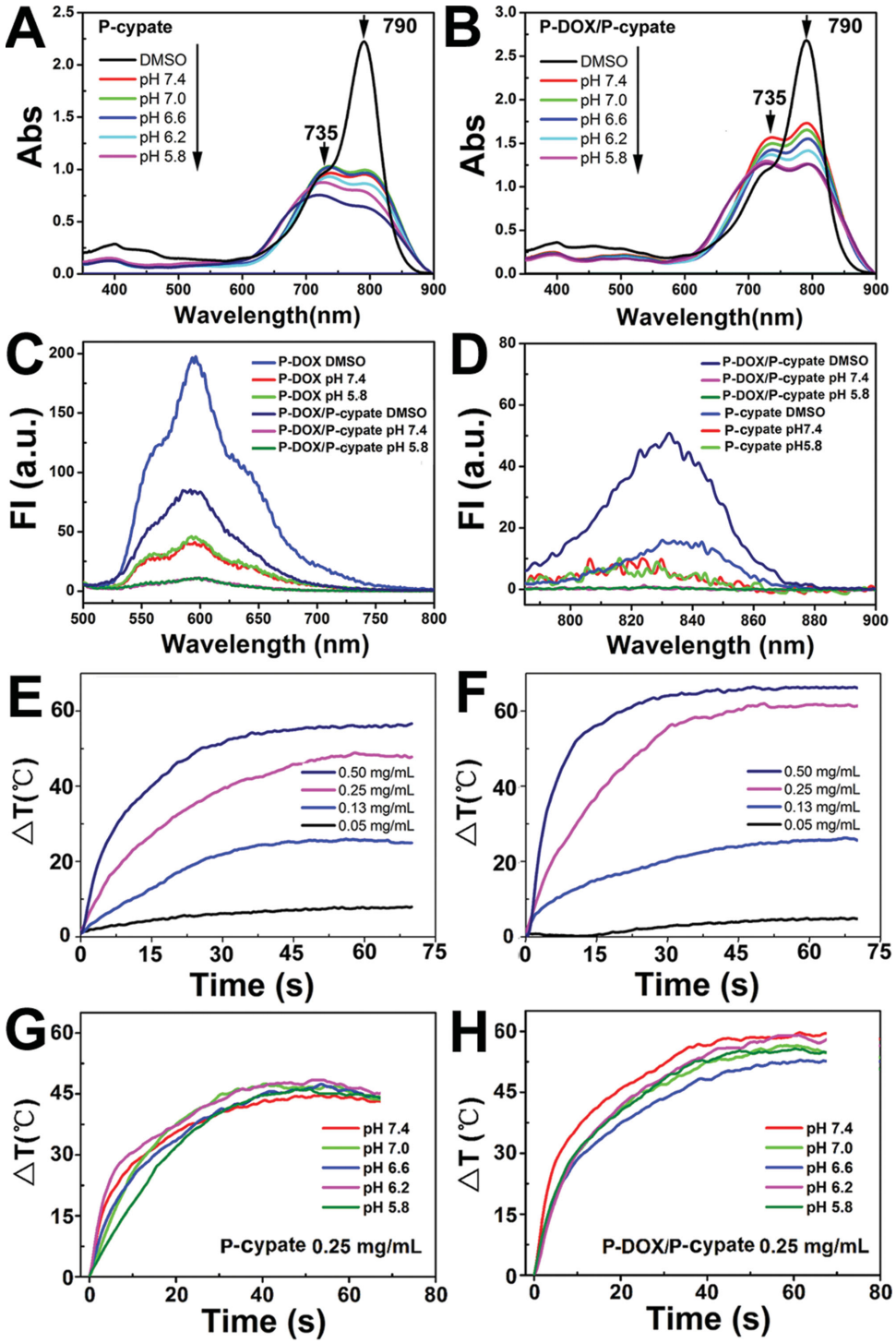

Figure 3. UV–vis and fluorescence spectra of A,C) P-cypate and B,D) P-DOX/P-cypate micelles, respectively. E–H) Concentration-dependent temperature elevation profiles of E) P-cypate and F) P-DOX/P-cypate micelles; photothermal effect of G) P-cypate and H) P-DOX/P-cypate micelles determined at various pH conditions.

at pH ≤ 6.2 as demonstrated in Figure 2. In the meanwhile, the A_{735}/A_{790} ratios of both P-cypate and P-DOX/P-cypate increased gradually when the buffer pH was reduced (Figure S4, Supporting Information), along with blue shifting of the absorption band, which might be caused by H-type aggregation of cypate at acidic pH due to its poor water solubility. Interestingly, P-DOX/P-cypate displayed stronger UV–vis absorbance than P-cypate alone at a same cypate concentration disregarding the buffer pH, implying that aggregation of cypate was partly inhibited by P-DOX loaded into P-cypate micelles due to diluted cypate

concentration inside the micelles. The fluorescence spectra of P-DOX and P-cypate were shown in Figure 3C,D, respectively. The fluorescence emission of P-DOX and P-cypate in P-DOX/P-cypate micelles was obviously quenched at pH 7.4, due to aggregation of P-DOX and P-cypate in the hydrophobic core of the hybrid micelles. The fluorescence emission of cypate was not recovered when the micelles dissociated at acidic pH of 5.8.

Given the broad absorbance while quenched fluorescence emission of P-DOX/P-cypate micelles in the 650–850 nm NIR region, we next evaluated the ability of P-DOX/P-cypate micelles to convert the absorbed photon into heat using 808 nm laser as photo source. We found that both P-DOX/P-cypate and P-cypate micelles induced significant temperature elevation in a cypate concentration-dependent manner (Figure 3E,F). The photothermal property of neither P-cypate nor P-DOX/P-cypate micelles was affected by changing buffer pH (Figure 3G,H). It was worth noting that P-DOX/P-cypate micelles caused higher temperature elevation than that of P-cypate micelles in the pH range from 5.8 to 7.4, which was most likely attributed to the stronger absorbance of P-DOX/P-cypate micelles over that of P-cypate ones (Figure 3A,B). All these results implied a good potential of P-DOX/P-cypate micelles to induce hyperthermia effect inside cells even they were dissociated in acidic lysosome vesicles upon intracellular uptake.

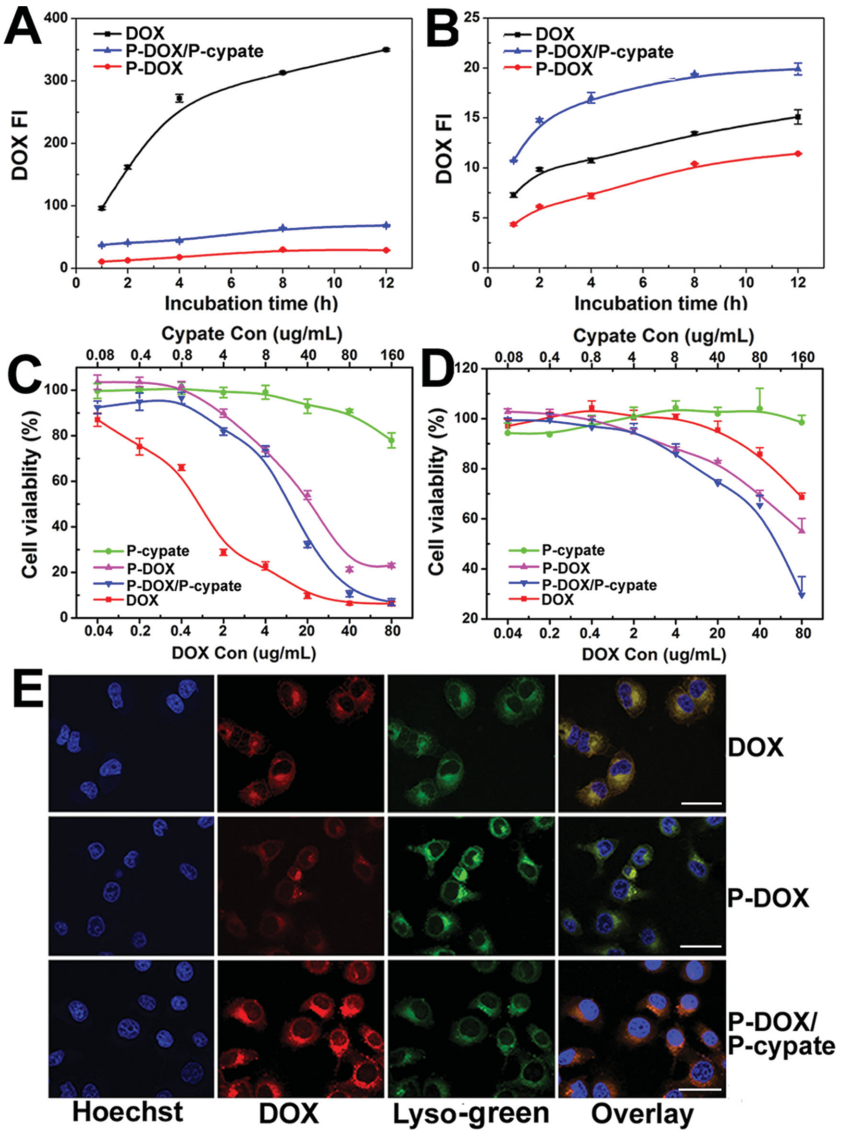

Figure 4. A,B) Quantitative analysis of DOX accumulation in A) MCF-7 or B) MCF-7/ADR cells after incubated with free DOX, P-DOX prodrug, or P-DOX/P-cypate micelles for various durations. An equal DOX dose of 10 μg mL^{-1} was used for both cellular uptake and distribution studies. C,D) Cytotoxicity assay of free DOX, P-DOX prodrug, or P-DOX/P-cypate hybrid micelles in C) MCF-7 and D) MCF-7/ADR cells. E) CLSM determined DOX distribution in MCF-7/ADR cells after coincubated with DOX, P-DOX prodrug, or P-DOX/P-cypate micelles for 12 h (scale bar 100 μm).

2.2. Cellular Uptake, Distribution, and Cytotoxicity of P-DOX/P-Cypate Micelles

To investigate whether P-DOX/P-cypate micelles could be internalized by the DOX-resistant breast cancer cells, we first measured the intracellular DOX concentration using a flow cytometric method. Much higher DOX concentration was found in DOX-treated parental MCF-7 cells than that in cells incubated with P-DOX/P-cypate micelles or P-DOX nanoparticles (**Figure 4**A) due to the high efficiency of diffusion-mediated uptake of free DOX. The trends were reversed in adriamycin-resistant MCF-7 (MCF-7/ADR) cells. Free DOX uptake in MCF-7/ADR cells was significantly suppressed due to P-gp protein-mediated efflux of DOX. Furthermore, 1.3-fold higher fluorescence intensity of DOX was found in cells treated with P-DOX/P-cypate micelles than that in cells treated with DOX, implying that P-DOX/P-cypate micelles could partly bypass the P-gp efflux pathway via endocytosis-mediated internalization (Figure 4B). Compared with P-DOX/P-cypate hybrid micelles, P-DOX treatment resulted in less DOX accumulation in both MCF-7 and MCF-7/ADR cells, implying lower internalization efficiency of P-DOX nanoparticles than that of P-DOX/P-cypate micelles. This could be presumably explained by the larger particle size of P-DOX nanoparticles than that of P-DOX/P-cypate micelles as shown in Figure 2A,E, since the endocytosis of nanoparticles was reported to be particle size-dependent, and the nanoparticles with a smaller hydrodynamic radius generally contributed to a higher intracellular uptake efficacy than the larger ones.[34,35]

We next evaluated the cytotoxicity of P-DOX/P-cypate micelles in both MCF-7 and MCF-7/ADR cells using sulforhodamine B (SRB) staining assay. As shown in Figure 4C, comparable cytotoxicity of free DOX, P-DOX, and P-DOX/P-cypate micelles was found in sensitive MCF-7 cells at high

DOX concentrations (i.e., >40 μg mL^{-1}), confirming the successful release of active DOX from P-DOX. However, P-DOX/P-cypate micelles showed low efficiency to reverse DOX resistance in MCF-7/ADR cells since the hybrid micelles displayed only a slightly higher cytotoxicity than that of free DOX (Figure 4D). The intracellular distribution of DOX in both MCF-7 and MCF-7/ADR cells was then observed using confocal laser scanning microscopic (CLSM) examination. In consistent with the flow cytometric data, higher DOX fluorescence intensity was found in MCF-7/ADR cells treated with P-DOX/P-cypate than that in cells incubated with free DOX. DOX inside the MCF-7/ADR cells was colocalized well with the lysosome vesicles without observable nucleus translocation (Figure 4E). In contrast, free DOX internalized in MCF-7 cells was mainly colocalized with cellular nucleus (Figure S5, Supporting Information). This phenomenon could be presumably explained by lysosome sequestration of DOX payload disregarding the formulations in MCF-7/ADR cells (i.e., free DOX or P-DOX in P-DOX/P-cypate micelles) since MDR cells contain increased number of lysosome vesicles.[21,23]

2.3. Hyperthermia-Triggered Cytoplasm DOX Release In Vitro

Given the high photothermal conversing efficiency of P-DOX/P-cypate micelles demonstrated in Figure 3E–H, their ability to induce intracellular hyperthermia effect was examined in MCF-7/ADR cells in vitro. To avoid the cytotoxicity of P-DOX/P-cypate micelles, P123/P-cypate micelles without P-DOX were used for temperature elevation studies in vitro. Before exposed to 808 nm laser illumination, the cells were preincubated with P-DOX/P-cypate micelles for 12 h to ensure sufficient cellular uptake of the micelles. The cells were then collected by centrifugation and finally resuspended in 50 μL of phosphate buffer solution (PBS) in Eppendorf tubes. As shown in **Figure 5**A,B, laser irradiation significantly induced the temperature elevation in both the laser power and micelle concentration-dependent manners. For example, a maximal temperature elevation (> 35 °C) was achieved at a cypate concentration of 200 μg mL^{-1} and laser intensity of 32 W cm^{-2}.

Since P123/P-cypate micelle induced tunable photothermal effect inside MCF-7/ADR, the hyperthermia-triggered cytoplasm DOX release was then exploited using CLSM method. To minimize hyperthermia-induced degradation of cytoskeleton proteins and the cellular necrosis, a moderate temperature elevation of 5–10 °C was carefully tuned by selecting a cypate concentration of 150 μg mL^{-1}, DOX concentration of 8 μg mL^{-1}, and laser intensity of 24 W cm^{-2}, respectively. As shown in Figure 5C, after exposed to laser light for 2 min, a highly diffused pattern of DOX distribution was observed, suggesting disruption of the lysosome membrane and cytoplasm release of DOX payload, which was further confirmed by the reduced colocalization between lysotracker green and DOX (Figure S6, Supporting Information). Moreover, the cells kept their morphology well after laser illumination, suggesting no obvious damage was caused on cellular membrane. The hyperthermia-enhanced cytoplasm DOX release induced higher cytotoxicity of P-DOX/P-cypate micelles. Over 50% of micelle-incubated MCF-7/ADR cells lost their viability when examined at 24 h postlaser illumination. In contrast, no notable decrease in cell survival rate was found in P-cypate and laser treated cells. The CLSM and phototoxicity data clearly suggested that moderate hyperthermia-triggered cytosol drug release could be a practicable strategy for circumventing cancer MDR, at least in cellular level.

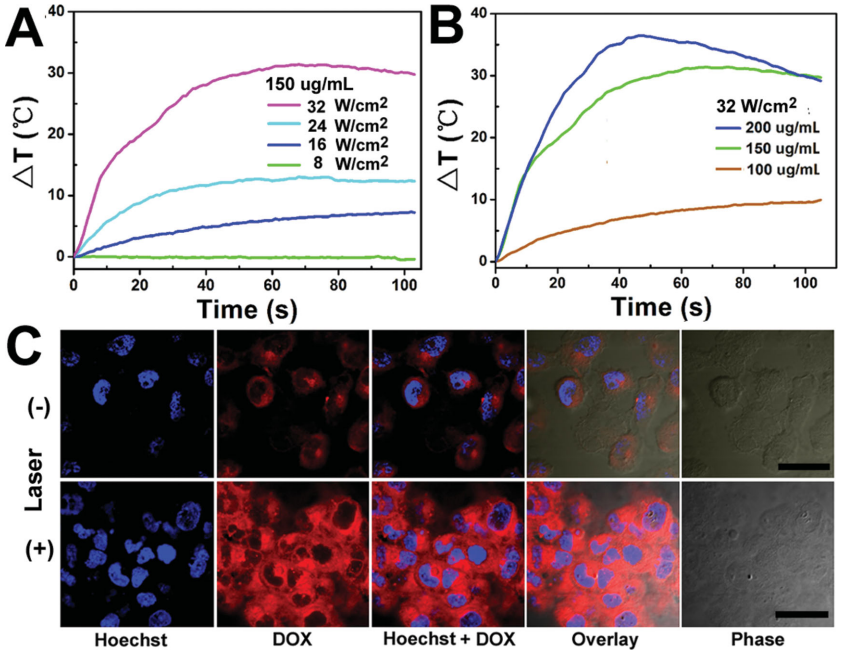

Figure 5. A) Laser power and B) micelle concentration-dependent photothermal effect of MCF-7/ADR cells incubated with P123/P-cypate micelles for 12 h (cypate concentration of 150 μg mL^{-1} and laser power output of 4.0 W was selected for temperature elevation studies, respectively). C) NIR-laser light triggered cytosol release of DOX payload in MCF-7/ADR cells, the cells were preincubated with P-DOX/P-cypate micelles at a cypate concentration of 150 μg mL^{-1} and DOX concentration of 7.5 μg mL^{-1}, respectively (scale bar 50 μm).

2.4. Biodistribution and Pharmacokinetics of P-DOX/P-Cypate Micelles In Vivo

It was reported that nanoparticles less than 5 nm could be quickly cleared off blood circulation through renal filtration.[36] Meanwhile, large nanoparticles with particle size over 200 nm were also susceptible to reticuloendothelial system (RES) clearance.[17] To evaluate the in vivo fate of our dual-responsive P-DOX/P-cypate micelles, an analog of P-DOX was synthesized by conjugating a NIR dye Ce6 onto P123 (denoted as P-Ce6) because Ce6 exhibited strong fluorescence emission in the NIR region (650–700 nm). The in vivo biodistribution of P-Ce6/P-cypate micelles was then investigated using fluorescence imaging examination. As shown in **Figure 6**A,B, the clear distribution of P-Ce6/PDPA micelles was found in xenograft

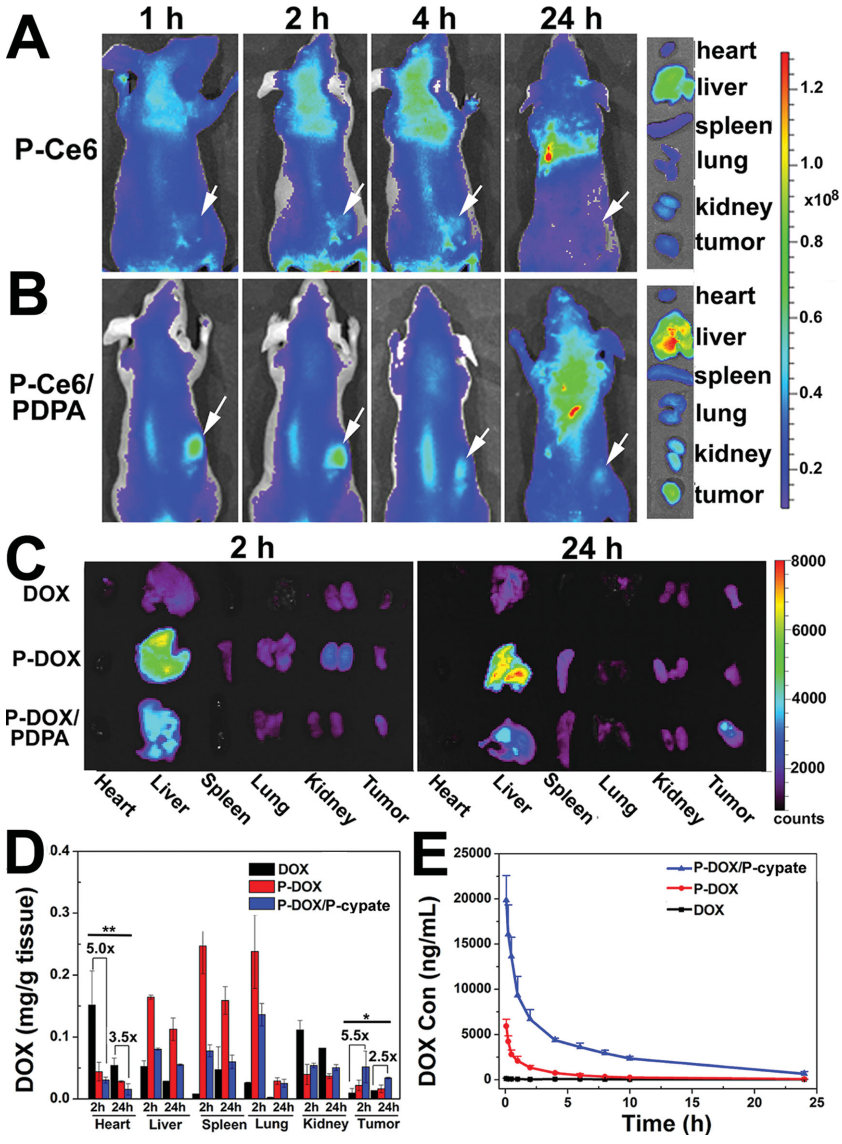

Figure 6. In vivo biodistribution of P123 A) and P123/PDPA B) micelles examined by fluorescent imaging at different time points post i.v. administration (the location of the xenograft tumor was indicated with the white arrows). C) Ex vivo DOX biodistribution in major organs examined 2 or 24 h post micelle administration. D) Quantitative analysis of DOX distribution in major organs examined at 2 or 24 h post i.v. injection (**, $P < 0.001$; *, $P < 0.05$). E) Plasma concentration of DOX versus time profiles in rats after intravenous administration of free DOX, P-DOX, or P-DOX/P-cypate micelle at a DOX dose of 5.0 mg kg^{-1}.

MCF-7/ADR tumor 1 h post tail vein intravenous (i.v.) injection. The fluorescence intensity increased further at 2 h and then dropped slowly over the time due to blood clearance of the micelles. Afterwards, the ex vivo biodistribution of P-DOX/P-cypate were examined in MCF-7/ADR xenograft tumor bearing mice using fluorescent imaging and fluorescent spectroscopic measurement, respectively. At 2 and 24 h time after systemic micelle administration, the major fraction of free DOX was found in heart, liver, and kidney, and distribution in tumor was negligible, implying quick clearance of free DOX by renal filtration and kupffer cells (Figure 6C). In contrast, P-DOX/P-cypate micelles displayed 5.5 and 2.5-magnitude higher intratumoral DOX concentrations than that of free DOX, respectively, which could be mainly attributed to the passive targeting tumor ability of P-DOX/PDPA micelles as revealed by the biodistribution study in vivo (Figure 6A). Notably, the heart distribution of DOX was also reduced by 4.8 and 5.9-folds respectively, when delivered with P-DOX/P-cypate micelles (Figure 6D). Furthermore, the pharmacokinetic of DOX was assessed using a Sprague Dawley (SD) rat model. As presented in Figure 6E and Table SI1, Supporting Information, P-DOX/P-cypate micelles significantly increased the maximal blood concentration (C_{max}) and the area under the curve ($AUC_{(0\text{-}t)}$) of DOX by 152 and 12.1-fold over that of free DOX, respectively. These data indicated a significant longer blood circulation time of P-DOX/P-cypate micelles than that of free DOX, which could be presumably attributed to their suitable particle size (≈30 nm) and neutral PEG corona to avoid renal filtration and escape RES clearance.

2.5. Hyperthermia-Triggered Tumor Penetration In Vivo

Encouraged by the passive tumor accumulation ability of P-DOX/P-cypate micelles, we next investigated their hyperthermia effect in vivo. The tumor-bearing mice were i.v. administrated with PBS, P-DOX, P-cypate, or P-DOX/P-cypate, respectively, and examined for laser-controlled temperature elevation at 2 h after i.v. injection. After illuminated with 808 nm NIR laser for 90 s, a moderate temperature increases of 15 and 20 °C were achieved in P-cypate and P-DOX/P-cypate injected mice, respectively. In obvious contrast with the slight tumoral temperature elevation (≈5 °C) in PBS or P-DOX-injected mouse (**Figure 7**A,B). The higher temperature increase observed in P-DOX/P-cypate-treated mouse than that of P-cypate-injected one could be explained by the better photothermal conversing efficacy of P-DOX/P-cypate micelles as demonstrated in Figure 3E–H. For a kinetic study of the hyperthermia effect in vivo, the xenograft tumors were illuminated with 808 nm laser at desired time points following micelle injection. The tumor temperature was increased by ≈20 °C when examined at 2 h after micelle injection, about 8 °C higher than that determined at 1 h (Figure 7C). The temperature elevation decreased gradually over the time (i.e., 4 or 24 h post micelle injection). This phenomenon was consistent with the in vivo biodistribution pattern of P-Ce6/P-cypate micelles. Thus, a positive correlation between the intratumoral micelle concentration and their hyperthermia effect could be established. The influence of

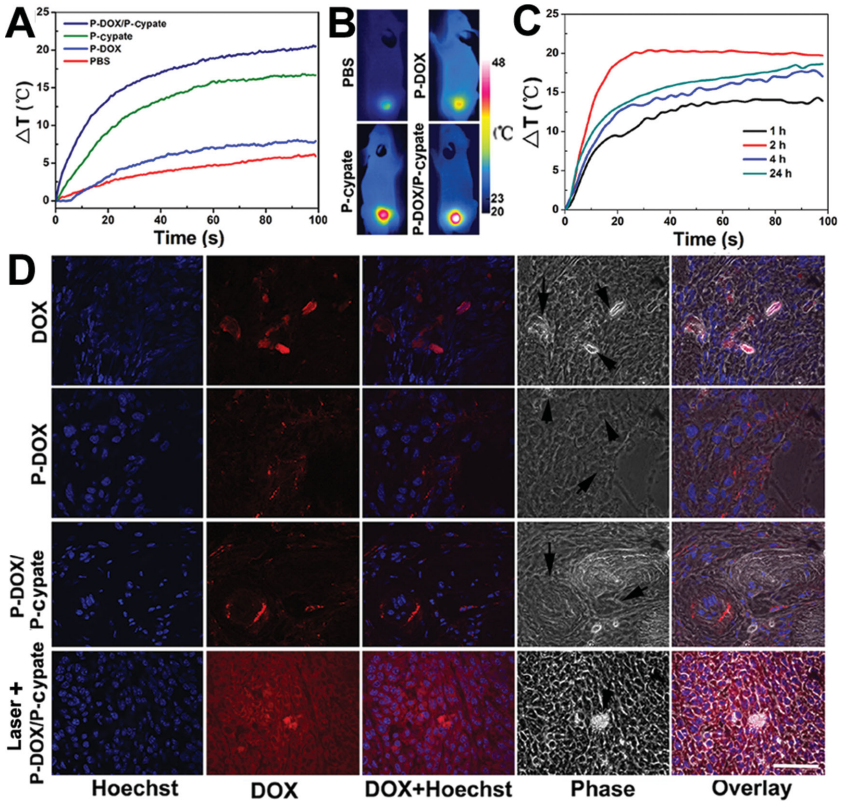

Figure 7. A) Laser irradiation induced temperature elevation and B) the thermographic images of tumor-bearing mice i.v. injected with PBS, P-DOX, P-cypate, or P-DOX/P-cypate micelles. C) Temperature elevation curves of tumor bearing mice i.v. injected with P-DOX/P-cypate micelles, the mice were treated with 808 nm laser (16 W cm^{-2}) at various time points after micelle injection. D) The NIR laser irradiation induced hyperthermia effect can obviously trigger tumor penetration of P-DOX loaded hybrid micelles (scale bar 100 μm).

cypate-induced hyperthermia on intratumor DOX distribution was further investigated by CLSM examination. Without laser treatment, DOX accumulated inside the tumor organ mainly distributed in the perivascular areas without notable deep tumor diffusion when administrated in the form of free DOX, P-DOX, or P-DOX/P-cypate micelles. This could be caused by the presence of the aforementioned extracellular barriers (i.e., high interstitial fluid pressure, reduced transcapillary pressure gradient, and dense extracellular matrix). Excitingly, after exposed to NIR laser irradiation for 2 min at laser intensity of 16 W cm^{-2}, a highly diffused DOX distribution pattern with bright fluorescence emission was observed. The DOX positive tumor area was also significantly improved from 50% to near 100% in comparison with that of P-DOX/P-cypate injected mock control. Strong DOX fluorescence was found surrounding the cellular nucleus, implying successful internalization of DOX penetrated into deep tumor. However, only a small fraction of DOX payload was colocalized with nuclei (see enlarged CLSM images in Figure S7, Supporting Information), indicating that intracellular trafficking of DOX to nuclei might be another cellular barrier for DOX delivery.[37]

2.6. Tumor Growth Inhibition and Biosafety In Vivo

Since P-DOX/P-cypate micelles could passively accumulated inside the xenograft tumors via "EPR" effect, and laser illumination following micelle administration could trigger the tumor penetration and cytoplasm release of DOX payload, we proceeded to evaluate the ability of P-DOX/P-cypate micelles to reverse DOX resistance in MCF-7/ADR breast cancer in vivo. In the group treated with PBS or P-cypate micelles, the tumors grew rapidly over 1500 mm^3 in 9 days post the first injection (**Figure 8**A). The tumor growth rate was suppressed by 30%–40% when treated with free DOX, P-DOX, or P-DOX/P-cypate micelles. Despite much higher tumoral DOX concentration was detected in P-DOX/P-cypate group than that in DOX or P-DOX group, no statistic difference of tumor growth rates was found among free DOX, P-DOX, and P-DOX/P-cypate groups, which might be caused by the limited tumor penetration of the hybrid micelles. When illuminated with a NIR laser following i.v. injection of P-DOX/P-cypate micelles, the growth of MCF-7/ADR tumor was completely inhibited in the whole therapy period, even only a moderate hyperthermia effect was

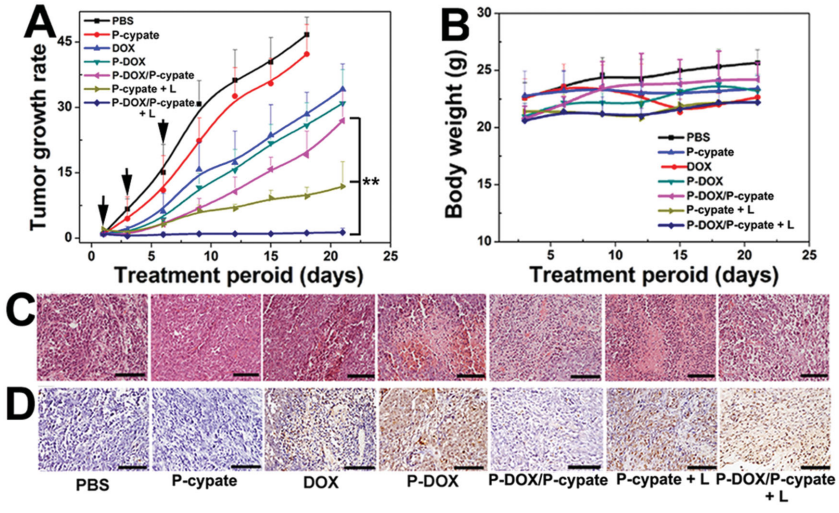

Figure 8. A) Tumor growth inhibition profiles of P-DOX/P-cypate micelles in combination with NIR laser irradiation in MCF-7/ADR tumor-bearing mice ($^{**}P < 0.001$), the black arrows indicated the time points for micelle administration. B) body weight change of tumor-bearing mice determined during the animal studies. C) H&E and D) tunnel staining assays of tumor organs collected at the end of tumor growth inhibition studies (scale bar 200 μm for all images).

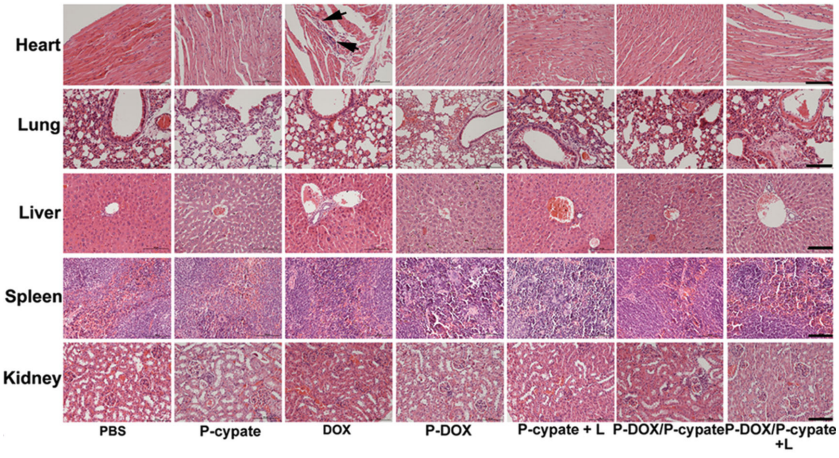

Figure 9. H&E staining assay of heart, lung, liver, spleen, and kidney collected at the end of tumor growth inhibition studies, the black arrows indicated the accumulation of neutrophils in the heart of DOX-treated mouse. Moreover, obvious myocardial damage was also found in the heart of DOX group (scale bar 100 μm for all images).

induced under this condition (≈20 °C). In contrast, the tumor growth rate of P-cypate plus laser group was eightfold higher than that of P-DOX/P-cypate plus laser group, implying hyperthermia-triggered tumor diffusion and cytosol release of DOX payload could significantly improve the antitumor efficacy of P-DOX/P-cypate. As an indirect indicator of systemic toxicity, the body weight change of all groups was monitored during the experiment. The body weight of saline group increased gradually, partly due to the fast growth of the xenograft tumor. Dramatic body weight loss was found for DOX group as compared with that of P-DOX/P-cypate or P-DOX/P-cypate + laser group, indicating better animal tolerance of P-DOX/P-cypate micelles than that of free DOX (Figure 8B). To understand the possible mechanism underlying for the superior antitumor ability of P-DOX/P-cypate + laser over that of free DOX or P-DOX/P-cypate, the tumor tissues were fixed and analyzed by hematoxylin–eosin (H&E) staining assay. Obvious DNA damage and membrane degradation were found in the tumor slices of P-DOX/P-cypate + laser over that of free DOX or P-DOX/P-cypate, the tumor tissues were fixed and analyzed by H&E staining assay. Obvious DNA damage and membrane degradation were found in the tumor slices of P-DOX/P-cypate + laser group, as compared with that of DOX or P-DOX/P-cypate group (Figure 8C). The tumor slices of each group were further examined by tunnel staining assay. The significant cellular apoptosis was detected in mouse group treated with P-DOX/P-cypate in combination with laser irradiation (Figure 8D).

All these results clearly demonstrated that the systemic administration of P-DOX/P-cypate micelles in combination with hyperthermia-triggered tumor penetration/cytosol release of DOX payload could synergistically override the DOX resistance in MCF-7/ADR cells. Histological studies showed obvious neutrophils accumulation in heart in DOX group (**Figure 9**), suggesting acute cardiotoxicity of free DOX. In contrast, no neutrophils accumulation was found in P-DOX or P-DOX/P-cypate group, most likely due to the reduced heart distribution of DOX as shown in Figure 5C. In addition to heart, no observable damage was found in other major organs (i.e., liver, spleen, lung and kidney) of P-DOX/P-cypate group, further confirmed good biocompatibility of P-DOX/P-cypate micelles.

To date, many nanoparticle drug delivery systems have been exploited to combat cancer MDR by coadministrating multichemotherapeutics,[38,39] or codelivering siRNA and anticancer drugs.[40,41] However, many of these nanoparticles are prepared by noncovalently encapsulating chemotherapeutic payloads inside the hydrophobic core, and unable to diffuse throughout the tumor mass for efficient drug delivery. In comparison with the conventional designs, the pH and NIR light dual-responsive micelles reported in this study had a couple of advantages. First, a polymeric prodrug of DOX was incorporated to increase the drug loading capacity and prevent drug leakage during systemic circulation. P123 released from the prodrug inhibited DOX efflux by suppressing P-gp activation. Moreover, cypate-conjugated pH-responsive mPEG-*b*-PDPA diblock copolymer could serve as both a photoabsorbent to convert NIR light into local heat and a pH-switchable carrier for P-DOX. At neutral pH, P-cypate copolymer could compress P-DOX into compact micellar nanoparticles (hydrodynamic diameter around 35 nm) for long blood circulation and passive tumor targeting. The micelles were specifically dissociated in weakly acidic organelles (pH 5.5–6.0) to release P-DOX payload. Upon illumination with 808 nm NIR laser, cypate-conjugated copolymer could induce moderate hyperthermia effect by efficiently converting the photo energy to local heat, thus facilitate the tumor penetration and cytosol release DOX payload by disrupting the dense extracellular matrix and lysosome membrane (Figure 1D).

The combination of plasmonic photothermal therapy with nanoparticulate or polymeric chemotherapeutics has recently been exploited to improve tumor accumulation and penetration of chemotherapeutics.[12,42] However, preinjection of gold nanorods was essential for such an approach, made it a little inferior to our "all-in-one" system. Photoswitchable nanoparticles were also reported by Kohane et al. to enhance the tumor delivery of chemotherapeutic payload,[18] but 365 nm UV light was required to trigger nanoparticle shrinkage via cleavage of covalent bond, which was the Achilles' heel of such a design due to the poor tissue penetration and severe side effect of short wavelength UV light. In contrast, the 808 nm NIR laser used herein has the obvious advantages of deep tissue transparence and low skin absorption. More importantly, the hyperthermia effect of P-DOX/P-cypate micelles could be readily tuned by adjusting P-cypate loading ratios and laser intensity since their temperature elevation property was directly dependents on cypate-concentration and laser power output.

A recent study reported by Chen et al. described a strategy to combat caner MDR in molecular level by localized plasmonic heating of gold nanorod at a mild laser power density to modulate the drug-resistance related genes.[43] The mild hyperthermia effect induced by laser irradiation was demonstrated to combat cancer MDR by triggering higher expression of heat

shock factor (HSF-1) trimers and down-regulate the expression of P-gp and mutant p53. On the contrary, our study demonstrated a new strategy to circumvent cancer MDR by targeting both the physiological and biological barriers (i.e., the limited nanoparticle penetration in tumor mass due to the dense stroma and high interstitial pressure of MDR tumor, and the increased number of lysosome vesicles in MDR cancer cells). The studies conducted by Chen et al. and us complementarily implied the promising potential of NIR-laser triggered mild hyperthermia for combating cancer MDR in organ, cell, and molecular levels.

3. Conclusion

A novel P-DOX/P-cypate hybrid micelle for combating DOX resistance in breast cancer was developed. The micelles displayed dual-responsiveness to both intracellular acidic pH and NIR light. At physiological condition, the micelles could compress DOX prodrug into compact nanostructure to prolong its blood circulation, which were while dissociated to release payload in weakly acidic intracellular environment. The hybrid micelles in combination with NIR laser irradiation induced tunable hyperthermia effect both in cellular and animal level. Localized NIR laser irradiation following systemic administration of the hybrid micelles could simultaneously triggered the deep tumor penetration and cytoplasm release of DOX payload, thus significantly improve the therapeutic efficacy of P-DOX/P-cypate micelles for treatment of DOX-resistant MCF-7/ADR breast cancer. Taken together, the results reported in this study might imply a novel approach to combat MDR breast cancer by targeting the biological barriers.

4. Experimental Section

Materials: Methoxy polyethylene glycol 5000 ($mPEG_{114}$-OH), copper bromide (CuBr), anhydrous *N*,*N*'-dimethylformamide (DMF), 2-hydroxyethyl methacrylate (HEMA), pentamethyldiethylenetriamine (PMDETA), pluronic copolymer P123 (EO_{20}-PO_{70}-EO_{19}), and succine anhydride were all ordered from Sigma-Aldrich (Shanghai, China) and used as received. 2-(Di-isopropylamino) ethyl methacrylate (DPA) was purchased from Scientific Polymer Products Inc. (Ontario, NY, USA) and purified by vacuum distillation over calcium hydride. Dialysis tubing with molecular weight cut-off (MWCO) of 3500 Da was ordered from Fisher Scientific. Inc. (IL, USA). NR fluorescence probe was purchased from MP Biomedicals, LLC. (Ohio, USA). LysoTracker green (DND-26) and Hoechst 33342 was obtained from Life Technologies (Shanghai, China). NH_2–GFLG–COOH tetrapeptide was synthesized by GL Biochem Co., Ltd (Shanghai, China). DOX hydrochloride was purchased from Shanwei Pharmaceutics Co., Ltd. (Shanghai, China). NIR fluorescence dye cypate was synthesized according to previous method.[44] The successful synthesis of cypate was confirmed by ^{1}H-NMR and mass spectrum examinations, respectively. Ce6-conjugated P123 (denoted as P-Ce6) was synthesized by coupling Ce6 on P123 via formation of ester bond between the carboxyl group of Ce6 and hydroxyl groups of P123.

Synthesis of P123 Conjugated DOX Prodrug (P-DOX): Free DOX was covalently conjugated to the end of P123 via an enzyme-cleavable tetrapeptide spacer of GFLG. To do that, the hydroxyl end groups of P123 were first converted to carboxyl groups by reacting with succine anhydride, and then functionalized with GFLG. Finally, DOX was conjugated with GFLG-P123 through coupling reaction between the carboxyl group of P123-GFLG and the amino group of DOX.

Synthesis of Cypate-Conjugated $mPEG_{113}$-b-P(DPA_{45}-r-$HEMA_3$) Diblock Copolymer (P-Cypate): $mPEG_{114}$-*b*-P(DPA_{40}-*r*-$HEMA_3$) diblock copolymer was synthesized by atom transfer radical polymerization method following the same procedure as reported in our previous work.[33] Afterwards, cypate was conjugated onto the pendant hydroxyl groups of $mPEG_{114}$-*b*-P(DPA_{45}-*r*-$HEMA_3$) diblock copolymer through coupling reaction between the carboxyl group of cypate and hydroxyl group of $mPEG_{114}$-*b*-P(DPA_{40}-*r*-$HEMA_3$) diblock copolymer. The chemical structure of the resultant product was examined by ^{1}H-NMR spectra using d6-DMSO as solvent. The weight percentage of cypate in the resultant copolymer was determined using UV–vis spectroscopic method.

Preparation and Characteristic of pH and NIR Light Dual-Responsive Micelles with P-DOX: P-DOX-loaded pH-responsive hybrid micelles were prepared using a solvent-evaporation method. Briefly, 8.6 mg of P-DOX and 11.4 mg of P-cypate (weight ratio of 43/57) were codissolved in 150 µL of anhydrous dimethylacetamide (DMAC), the resultant homogenous solution was added into 1.4 mL of distilled (DI) water under sonication. The P-DOX and P-cypate coloaded hybrid micelles (denoted as P-DOX/P-cypate) with DOX and cypate loading ratio of 3.4 and 6.8 wt%, respectively, were obtained after removing the organic solvent by dialyzing against DI water overnight. The pH-responsive property of P-DOX loaded P-DOX/P-cypate micelles was thoroughly characterized by measuring the change of size distribution and zeta potential versus medium pH by DLS measurement using a Nanosizer instrument at wavelength of 633 nm (ZS90, Malvern, UK). To investigate acidic pH-triggered dissociation of P-DOX/P-cypate micelles, 0.5 wt% of NR was loaded in P-DOX/PDPA micelles following the same procedure described above. The fluorescence images of NR-loaded micelles at different pH conditions were collected using an UVP Bioimage system (Upland, CA). The fluorescence spectrum of NR, DOX, and cypate were recorded with different wavelength setups (NR: Ex 475 nm, Em 500–800 nm; DOX: Ex 485 nm, Em 500–800 nm; cypate: Ex 750 nm, Em 760–900 nm, respectively, Hitachi F-4600, Japan). The morphology of the hybrid micelles was examined using TEM measurement (Joel, Japan). The light-responsive property of the hybrid micelles was evaluated using an 808 nm laser (Changchun New Industries Optoelectronics Tech. Co., Ltd, Changchun, China). The temperature change curves were recorded using an IR camera (IRTech Co. Ltd., Shanghai, China).

Cell Lines and Animals: Parental MCF-7 human breast cancer cell line was obtained from cell bank of Chinese Academy of Sciences (Shanghai, China). DOX-resistant MCF-7 cell line (MCF-7/ADR) was purchased from Keygen Biotech Co. Ltd (Shanghai, China). MCF-7 cells were cultured in complete RPMI 1640 cell culture medium containing 10% of fetal bovine serum, 100 U mL^{-1} of penicillin G sodium and 100 mg mL^{-1} of streptomycin sulfate. MCF-7/ADR cells were maintained in the similar culture medium used for MCF-7 cells with addition of 1.0 µg mL^{-1} of DOX. Both kinds of cells were maintained in 37 °C incubators under a humidified atmosphere with 5% CO_2 supply. All experiments were performed in the logarithmic phase of cell growth. All animals (i.e., SD rats and Balb/c nude mice) were purchased from Shanghai Experimental Animal Center (Shanghai, China). All animal procedures were carried out under the guidelines approved by the Institutional Animal Care and Use Committee (IACUC) of the Shanghai Institute of Material Medica, Chinese Academy of Sciences.

Cellular Uptake, Distribution, and Cytotoxicity of P-DOX/PDPA Hybrid Micelles: To investigate the cellular distribution of DOX-loaded micelles, MCF-7/ADR cells were seeded onto a round glass coverslips (Ø10 mm) in 24-well tissue culture plate at a density of 5×10^4 cells per well. After 24 h preincubation, the cells were treated with DOX, P-DOX, or P-DOX/P-cypate solution for 6 h at an equivalent DOX concentration of 10 µg mL^{-1}. Afterwards, the cells were stained with Hoechst 33342, washed with PBS, mounted with antifade solution and imaged using a confocal laser scanning microscopy (CLSM, Olympus Fluoview 1000, Japan). The acidic endocytosis organelles (i.e., late endosomes/lysosomes) were stained with lysotacker-green (DND-26, Life Tech, USA) 1 h before image taking. To quantitatively examine the cellular uptake of P-DOX/PDPA micelles, MCF-7 or MCF-7/ADR cells were both seeded

into 24-well tissue culture plates at a density of 2.0×10^5 cells per well. After 24 h preincubation, the cells were treated with DOX, P-DOX, or P-DOX/PDPA solutions for different time (i.e., 1, 2, 4, 8, and 12 h) at a DOX concentration of 10 μg mL^{-1}. Afterwards, the cellular fluorescence intensity of DOX was measured using a flow cytometry and the data were analyzed with a Cell Quest software. The cytotoxicity of P-DOX/P-cypate hybrid micelles was determined by SRB staining assay. Parental MCF-7 or MCF-7/ADR cells were seeded into 96-well tissue culture plate at a density of 1×10^4 cells per well in 100 μL of cell culture medium. The cells reached a confluence of 60%–80% after 24 h incubation. The cells were then incubated with free DOX, P-DOX, or P-DOX/P-cypate micelles at different DOX concentrations. After 48 h incubation, the cell viability was evaluated by SRB staining assay and expressed as relative cell viability after normalized with that of the untreated cell controls.

Photothermal Effect of P-DOX/P-Cypate Micelles and Laser-Triggered DOX Release In Vitro: MCF-7/ADR cells were seeded in six-well plates at a density of 2.0×10^5 cells per well, the cells were then preincubated with P123/P-cypate micelles for 12 h at three different cypate concentrations of 100, 150, and 200 μg mL^{-1}, respectively. Afterwards, the cells were thoroughly washed with PBS to remove any micelles attached on cell surface, centrifuged and redispersed in 50 μL of cell culture medium. The cell suspension was then illuminated with 808 nm NIR laser for 2 min at different laser power outputs (i.e., 16, 24, or 32 W cm^{-2}). The laser irradiation induced temperature elevation in vitro was recorded with an IR camera. To quantitatively determine the influence of cypate-induced hyperthermia effect on the viability of MCF-7/ADR cells, the cells were seeded in six-well plates at a density of 2.0×10^5 cells per well. After 24 h preincubation, the cells were treated with free DOX, P-cypate micelles, P-DOX, and P-DOX/P-cypate micelles for 12 h at an equivalent DOX or cypate concentration of 2.5 or 6.6 mg mL^{-1}, respectively. Afterwards, the cells were carefully washed with PBS, centrifuged, redispersed in 50 μL of cell culture medium and illuminated with an 808 nm laser for 2 min at different laser power outputs. The cells viability was then examined with SRB staining assay 24 h postlaser illumination.

Biodistribution and Pharmacokinetics of P-DOX/P-Cypate Hybrid Micelles In Vivo: To investigate the biodistribution of P-DOX/P-cypate micelles in vivo, DOX in the P-DOX copolymer was replaced with a porphorin dye Ce6 due to its strong fluorescence emission in the NIR region (650–700 nm). The biodistribution of P-Ce6/P-cypate micelles in vivo was then examined using a MCF-7/ADR tumor bearing Balb/c nude mouse model. To establish the orthotopic tumor model, each nude mouse (female, 4–5 weeks, 18 ± 2 g) was injected with 5.0×10^6 of MCF-7/ADR cells on the right mammary gland. After tumor volume reached 200 mm^3, the tumor-bearing mice were randomly grouped (n = 3), and intravenously injected with 200 μL of P-Ce6 or P-Ce6/P-cypate micelle at a Ce6 dose of 2.5 mg kg^{-1}. The whole body fluorescence images were collected at 1, 2, 4, or 24 h after micelle injection using a Caliper IVIS Lumina II in vivo imaging system (Perkin Elmer, USA). The mice were sacrificed at 24 h after micelle administration for ex vivo examining the micelle distribution in major organs. For quantitative analysis of DOX distribution in major tissues, the MCF-7/ADR tumor-bearing nude mice were randomly grouped (n = 3) and intravenously injected with free DOX, P-DOX, or P-DOX/P-cypate at an equal DOX dose of 5.0 mg kg^{-1}. The mice were sacrificed at 2 or 24 h after injection. All major organs (i.e., heart, liver, spleen, lung, kidney, and tumor) were weighted after fluorescence imaging, homogenized in 0.4 mL of methanol, and centrifuged at 10 000 rpm for 10 min to remove any supernatant. The DOX content in each tissue was then measured using a fluorescence spectrophotometric method and expressed as DOX weight in per gram of tissue. To investigate the pharmacokinetics of DOX, 1.0 mL of free DOX, P-DOX, and P-DOX/P-cypate solution with an equivalent DOX concentration of 5.0 mg mL^{-1} was intravenously injected to SD rats (female, 200–230 g, Shanghai Experimental Animal Center, Shanghai, China). Blood samples were collected at 5, 15, and 30 min and 1, 2, 4, 6, 12, and 24 h postadministration, the DOX concentration at each time point was determined using fluorescence spectrum measurement.

Photothermal Effect and Tumor Growth Inhibition In Vivo: The tumor growth inhibition experiment was conducted using nude mouse model bearing an orthotopicly implanted MCF-7/ADR tumor as that used for biodistribution study. The mice bearing MCF-7/ADR tumors of 50 mm^3 were randomly grouped into seven groups (n = 6) and intravenously injected with 100 μL of PBS, free DOX, P-cypate, P-DOX, and P-DOX/P-cypate at an equal DOX or cypate dose of 5.0 or 10 mg kg^{-1}, respectively. Two hours later after micelle injection, the tumors were locally irradiated by 808 nm NIR laser at a laser power output of 16 W cm^{-2} for 2 min (Changchun New Industries Optoelectronics Tech. Co., Ltd, Changchun, China). The temperature elevation of micelle injected tumor was recorded with the IR camera thermographic system. The treatment was repeated for three times at a time interval of 2 days. The tumor proliferation rates were monitored twice a week with a digital caliper and the body weights were examined using an electronic balance, respectively. The tumor volume was calculated by following formula: $V = (L \times W \times W)/2$ (L, longest dimension; W, shortest dimension) and expressed as relative tumor growth rate by normalizing with the initial tumor volume. The mice with tumor volume over 2000 mm^3 were euthanized and considered as animal death according to the animal protocol. All mice were sacrificed at 21 days post first micelle administration. The major organs (heart, liver, spleen, lung, kidney, and tumor) were collected and fixed with paraformaldehyde, dehydrated and sliced for H&E or immunohistological chemistry tunnel staining assay.

Statistical Analysis: Data were expressed as mean ± SD, the statistical significance was determined by using the one way analysis of variance. $p < 0.05$ was considered as significant.

Supporting Information

Supporting Information is available from the Wiley Online Library or from the author.

Acknowledgements

H.Y., Z.C., and P.Y. contributed equally to this work. Financial supports from the National Basic Research Program of China (2013CB932704 and 2012CB932502), the National Natural Science Foundation of China (81373359 and 81270047), and the SA-SIBS Scholarship Program are gratefully acknowledged.

Received: December 18, 2014
Revised: February 18, 2015
Published online: March 16, 2015

[1] D. E. Ziogas, *Curr. Oncol.* **2012**, *19*, 131.
[2] K. N. Abdullah, R. Janardhan, M. Hwang, C. D. Williams, M. Farasatpour, J. A. Margenthaler, K. S. Virgo, F. E. Johnson, *Am. J. Surg.* **2015**, *209*, 378.
[3] D. L. Hershman, J. Tsui, J. Meyer, S. Glied, G. C. Hillyer, J. D. Wright, A. I. Neugut, *J. Natl. Cancer Inst.* **2014**, *106*, dju319.
[4] S. G. Aller, J. Yu, A. Ward, Y. Weng, S. Chittaboina, R. Zhuo, P. M. Harrell, Y. T. Trinh, Q. Zhang, I. L. Urbatsch, G. Chang, *Science* **2009**, *323*, 1718.
[5] M. M. Gottesman, T. Fojo, S. E. Bates, *Nat. Rev. Cancer* **2002**, *2*, 48.
[6] A. M. Calcagno, C. D. Salcido, J. P. Gillet, C. P. Wu, J. M. Fostel, M. D. Mumau, M. M. Gottesman, L. Varticovski, S. V. Ambudkar, *J. Natl. Cancer Inst.* **2010**, *102*, 1637.
[7] M. R. Junttila, F. J. de Sauvage, *Nature* **2013**, *501*, 346.
[8] Y. C. Wang, M. S. Shim, N. S. Levinson, H. W. Sung, Y. N. Xia, *Adv. Funct. Mater.* **2014**, *24*, 4206.
[9] Q. Yin, J. N. Shen, Z. W. Zhang, H. J. Yu, Y. P. Li, *Adv. Drug Delivery Rev.* **2013**, *65*, 1699.
[10] M. E. Davis, Z. G. Chen, D. M. Shin, *Nat. Rev. Drug Discovery* **2008**, *7*, 771.

[11] X. J. Liang, H. Meng, Y. Wang, H. He, J. Meng, J. Lu, P. C. Wang, Y. Zhao, X. Gao, B. Sun, C. Chen, G. Xing, D. Shen, M. M. Gottesman, Y. Wu, J. J. Yin, L. Jia, *Proc. Natl. Acad. Sci. USA* **2010**, *107*, 7449.
[12] C. E. Ashley, E. C. Carnes, G. K. Phillips, D. Padilla, P. N. Durfee, P. A. Brown, T. N. Hanna, J. Liu, B. Phillips, M. B. Carter, N. J. Carroll, X. Jiang, D. R. Dunphy, C. L. Willman, D. N. Petsev, D. G. Evans, A. N. Parikh, B. Chackerian, W. Wharton, D. S. Peabody, C. J. Brinker, *Nat. Mater.* **2011**, *10*, 389.
[13] A. R. Kirtane, S. M. Kalscheuer, J. Panyam, *Adv. Drug Delivery Rev.* **2013**, *65*, 1731.
[14] T. L. Doane, C. Burda, *Chem. Soc. Rev.* **2012**, *41*, 2885.
[15] L. Bildstein, C. Dubernet, P. Couvreur, *Adv. Drug Delivery Rev.* **2011**, *63*, 3.
[16] Q. Sun, X. Sun, X. Ma, Z. Zhou, E. Jin, B. Zhang, Y. Shen, E. A. Van Kirk, W. J. Murdoch, J. R. Lott, T. P. Lodge, M. Radosz, Y. Zhao, *Adv. Mater.* **2014**, *26*, 7615.
[17] M. J. Ernsting, M. Murakami, A. Roy, S. D. Li, *J. Controlled Release* **2013**, *172*, 782.
[18] R. Tong, H. H. Chiang, D. S. Kohane, *Proc. Natl. Acad. Sci. USA* **2013**, *110*, 19048.
[19] H. Cabral, Y. Matsumoto, K. Mizuno, Q. Chen, M. Murakami, M. Kimura, Y. Terada, M. R. Kano, K. Miyazono, M. Uesaka, N. Nishiyama, K. Kataoka, *Nat. Nanotechnol.* **2011**, *6*, 815.
[20] C. Wong, T. Stylianopoulos, J. Cui, J. Martin, V. P. Chauhan, W. Jiang, Z. Popovic, R. K. Jain, M. G. Bawendi, D. Fukumura, *Proc. Natl. Acad. Sci. USA* **2011**, *108*, 2426.
[21] A. De Milito, S. Fais, *Future Oncol.* **2005**, *1*, 779.
[22] B. A. Webb, M. Chimenti, M. P. Jacobson, D. L. Barber, *Nat. Rev. Cancer* **2011**, *11*, 671.
[23] M. Schindler, S. Grabski, E. Hoff, S. M. Simon, *Biochemistry* **1996**, *35*, 2811.
[24] S. M. Simon, *Drug Discovery Today* **1999**, *4*, 32.
[25] H. Yu, Y. Zou, Y. Wang, X. Huang, G. Huang, B. D. Sumer, D. A. Boothman, J. Gao, *ACS Nano* **2011**, *5*, 9246.
[26] H. Yu, Y. Zou, L. Jiang, Q. Yin, X. He, L. Chen, Z. Zhang, W. Gu, Y. Li, *Biomaterials* **2013**, *34*, 2738.
[27] H. Yu, Z. Xu, X. Chen, L. Xu, Q. Yin, Z. Zhang, Y. Li, *Macromol. Biosci.* **2014**, *14*, 100.
[28] E. Batrakova, S. Lee, S. Li, A. Venne, V. Alakhov, A. Kabanov, *Pharm. Res.* **1999**, *16*, 1373.
[29] E. V. Batrakova, S. Li, S. V. Vinogradov, V. Y. Alakhov, D. W. Miller, A. V. Kabanov, *J. Pharmacol. Exp. Ther.* **2001**, *299*, 483.
[30] K. Ulbrich, J. Strohalm, V. Subr, D. Plocova, R. Duncan, B. Rihova, *Macromol. Symp.* **1996**, *103*, 177.
[31] D. Putnam, J. Kopecek, *Adv. Polym. Sci.* **1995**, *122*, 55.
[32] M. Guo, J. Huang, Y. Deng, H. Shen, Y. Ma, M. Zhang, A. Zhu, Y. Li, H. Hui, Y. Wang, X. Yang, Z. Zhang, H. Chen. *Adv. Funct. Mater.* **2014**,*25*, 59.
[33] H. Yu, Z. Xu, D. Wang, X. Chen, Z. Zhang, Q. Yin, Y. Li. *Polym. Chem.* **2013**, *4*, 5052.
[34] S. Zhang, J. Li, G. Lykotrafitis, G. Bao, S. Suresh. *Adv. Mater.* **2009**, *21*, 419.
[35] R. K. Jain, T. Stylianopoulos, *Nat. Rev. Drug Discovery* **2010**, *9*, 615.
[36] H. S. Choi, W. Liu, P. Misra, E. Tanaka, J. P. Zimmer, B. Itty Ipe, M. G. Bawendi, J. V. Frangioni, *Nat. Biotech.* **2007**, *25*, 1165.
[37] K. S. Soppimath, L. H. Liu, W.-Y. Seow, S.-Q. Liu, R. Powell, P. Chan, Y.-Y. Yang, *Adv. Funct. Mater* **2007**, *17*, 362.
[38] X. Xiong, A. Lavasanifar, *ACS Nano* **2011**, *5*, 5202.
[39] C. M. Hu, L. F. Zhang, *Curr. Drug Metab.* **2009**, *10*, 836.
[40] A. M. Chen, M. Zhang, D. Wei, D. Stueber, O. Taratula, T. Minko, H. He, *Small* **2009**, *5*, 2673.
[41] T. Fatemian, I. Othman, E. H. Chowdhury, *Drug Discovery Today* **2014**, *19*, 71.
[42] A. J. Gormley, N. Larson, S. Sadekar, R. Robinson, A. Ray, H. Ghandehari, *Nano Today* **2012**, *7*, 158.
[43] L. Wang, X. Lin, J. Wang, Z. Hu, Y. Ji, S. Hou, Y. Zhao, X. Wu, C. Chen, *Adv. Funct. Mater.* **2014**, *24*, 4229.
[44] Y. Ye, W. Li, C. J. Anderson, J. Kao, G. V. Nikiforovich, S. Achilefu, *J. Am. Chem. Soc.* **2003**, *125*, 7766.